Supplementary Information

Handcuff-like Metallo-Pseudorotaxanes Consisting of Tiara[5]arene Wheels and Dimeric Silver Trifluoroacetate Axles

Weiwei Yang,[a] Haiying Wang,[a] Rong Chang,[b] Zhitao Feng,[c] Yumei Zhu[a] and Andrew C.-H. Sue*[b]

[a] School of Pharmaceutical Science and Technology, Tianjin University, 92 Weijin Rd., Nankai Dist., Tianjin 300072, China.
[b] College of Chemistry and Chemical Engineering, Xiamen University, 422 Siming S. Rd., Siming Dist., Xiamen, Fujian Providence 361005, China.
[c] Department of Chemistry, University of California Davis, Davis, California 95616, United States.
*Corresponding author E-mail addresses: andrewsue@xmu.edu.cn

Table of Contents

1. General Methods

Starting materials, reagents, and solvents were purchased from commercial vendors and used as received without further purification. All compounds employed in this study were synthesized by following literature procedures unless otherwise noted. ^{1}H spectra were recorded on Bruker Advance 400 MHz spectrometer at ambient temperature. The chemical shifts are listed in ppm on the δ scale and coupling constants were recorded in Hz. Chemical shifts are calibrated relative to the signals of the non-deuterated solvents ($CHCl_3$: δ 7.26 ppm, CH_3OH: δ 3.31 ppm, $(CH_3)_2CO$, δ 2.05 ppm).

High-resolution mass spectra (HRMS) were measured on a Q-Exactive™ HF/UltiMate™ 3000 RSLCnano using a Nano ProFlow meter with ProFlow technology in the positive mode.

Single crystals suitable for X-ray diffraction were selected and mounted in inert oil in cold gas stream and their X-ray diffraction intensity data was collected on a Rigaku XtaLAB FRX diffractometer equipped with a Hypix6000HE detector, using Cu $K\alpha$ radiation (λ = 1.54184 Å). Crystals were kept at the temperature listed in **Table S1–S3** during data collection. The structures were solved either (i) with the ShelXS[1] structure solution program using Direct Methods or (ii) with the ShelXT[2] structure solution program using Direct Methods or Intrinsic Phasing and followed by refinement on F^2 by full-matrix least squares using Olex2[3] platform. The hydrogen atoms were set in calculated positions and refined as riding atoms with a common fixed isotropic thermal parameter. Selected details of the data collection and structural refinement of each compound can be found within **Table S1–S3** and full details are available in the corresponding CIF files. Crystallographic data (excluding structure factors) have been deposited with the Cambridge Crystallographic Data Centre (CCDC number: 2213177–2213179).

The electronic circular dichroism (ECD) spectra were recorded on a MOS-500 spectrophotometer. Solid state samples were prepared using the KBr pellet technique (40 mg of KBr per single crystal sample, finely ground), and then mounted on a pellet sample holder. The spectra were recorded in the range from 500 to 190 nm, with a step size of 1 nm, a bandwidth of 4 nm, a step of 1 s, and an acquisition period of 0.05 s.

2. NMR Studies

The silver trifluoroacetate (CF_3CO_2Ag) salt was obtained from commercial source and used as received without further purification. ^{1}H NMR titrations were performed in a mix solvent of $CDCl_3$ and $(CD_3)_2CO$ (v/v = 1:2) at ambient temperature by adding incremental amount of CF_3CO_2Ag into the macrocyclic host (**P[5]**[4], **T[5]**[5], and **[1$_5$]PCP**[6]) solutions (5 mM), respectively. In each titration experiment, up to 10 equiv. of CF_3CO_2Ag were added. Changes in chemical shift ($\Delta\delta$) of ^{1}H NMR signals of **P[5]** aromatic protons (H_1 and H_1*) and **T[5]** aromatic protons (H_p, H_o, and H_m) were recorded.

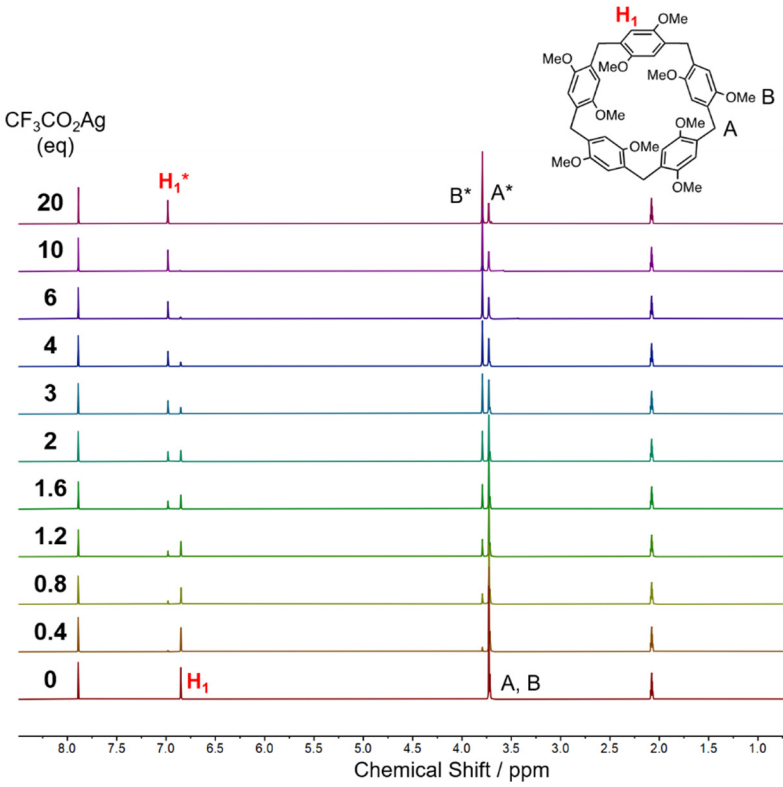

Figure S1. ^{1}H NMR spectra (400 MHz, $CDCl_3$: $(CD_3)_2CO$ = 1:2, v/v, 298 K) of **P[5]** at a concentration of 5 mM upon titration of CF_3CO_2Ag.

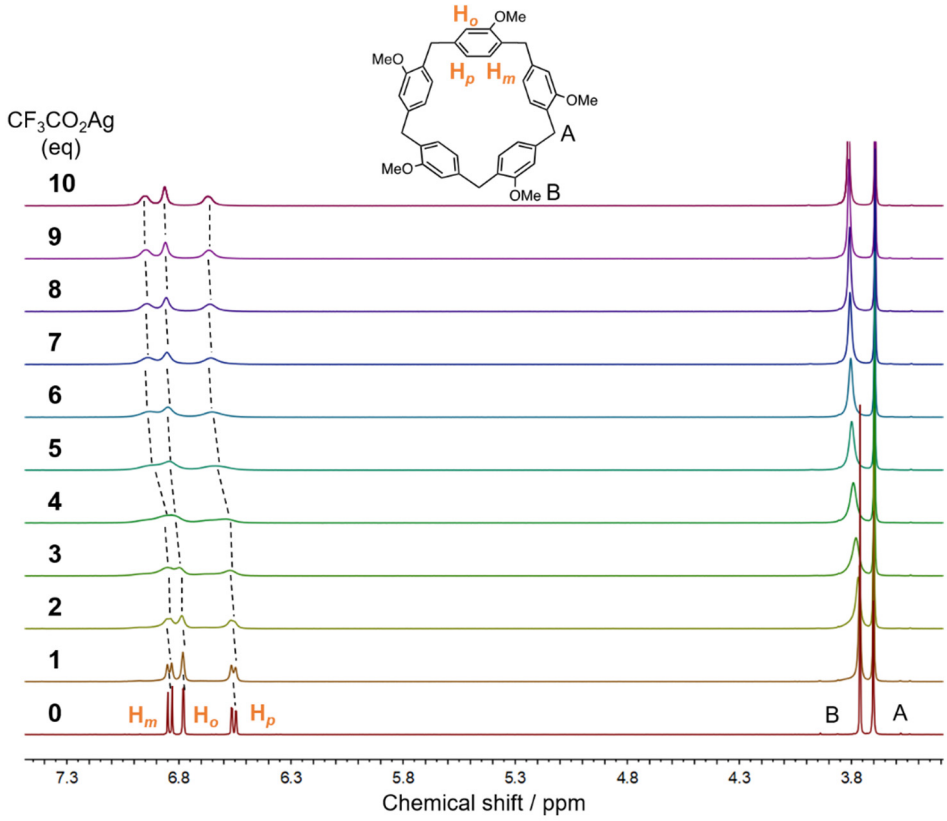

Figure S2. Partial ^{1}H NMR spectra (400 MHz, $CDCl_3$: $(CD_3)_2CO$ = 1:2, *v*/*v*, 298 K) of **T[5]** at a concentration of 5 mM upon titration of CF_3CO_2Ag.

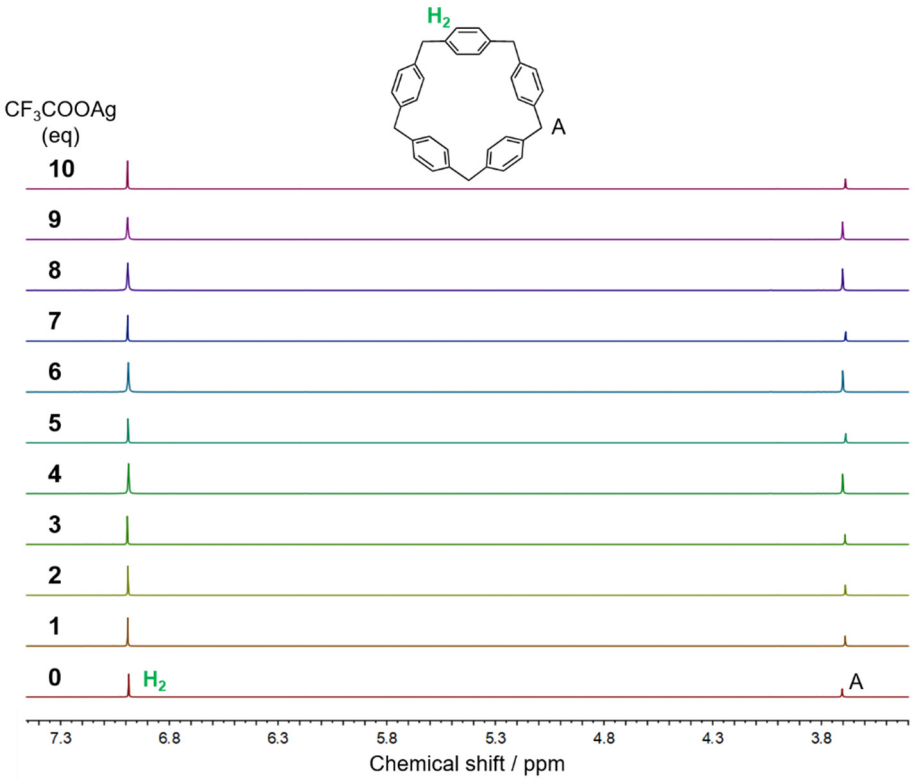

Figure S3. Partial ^{1}H NMR spectra (400 MHz, $CDCl_3$: $(CD_3)_2CO$ = 1:2, *v*/*v*, 298 K) of **[1$_5$]PCP** at a concentration of 5 mM upon titration of CF_3CO_2Ag.

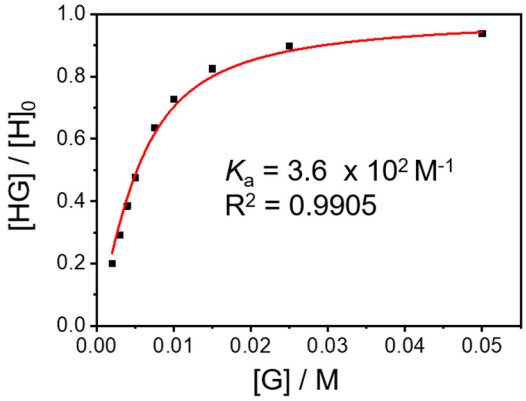

Figure S4. Data fitting for the titration of the $(CF_3CO_2Ag)_2$ guest into a solution of **P[5]**. To simplify the calculation process, the $(CF_3CO_2Ag)_2$ dimer is treated as one single guest species. The association constant K_a was estimated to be 3.6×10^2 M^{-1}.

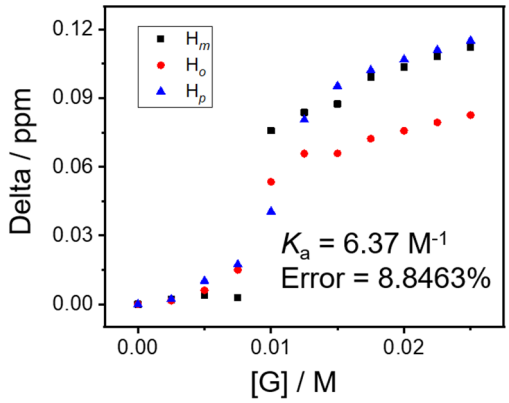

Figure S5. NMR titration curves of **T[5]** and the $(CF_3CO_2Ag)_2$ guest. Titration curve-fitting and association constant value were calculated by employing the BindFit program.[7] To simplify the calculation process, the $(CF_3CO_2Ag)_2$ dimer is treated as one single guest species. The association constant K_a was estimated to be 6.37 M^{-1}.

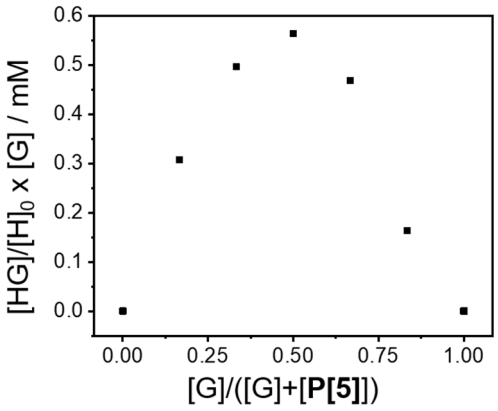

Figure S6. Job plots of the complexation between **P[5]** and the $(CF_3CO_2Ag)_2$ guest based on the ^1H NMR integrals of the host H_1 and H_1* proton signals. [**P[5]**] and [G] are concentrations of **P[5]** and the $(CF_3CO_2Ag)_2$ guest, respectively. [**P[5]**] + [G] = 6.0 mM.

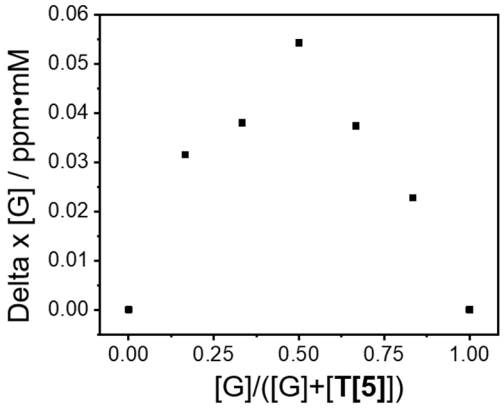

Figure S7. Job plots of the complexation between **T[5]** and the $(CF_3CO_2Ag)_2$ guest based on the chemical shift changes of the host proton signal in the ^{1}H NMR spectrum. [**T[5]**] and [G] are concentrations of **T[5]** and $(CF_3CO_2Ag)_2$ guest, respectively. [**T[5]**] + [G] = 6.0 mM.

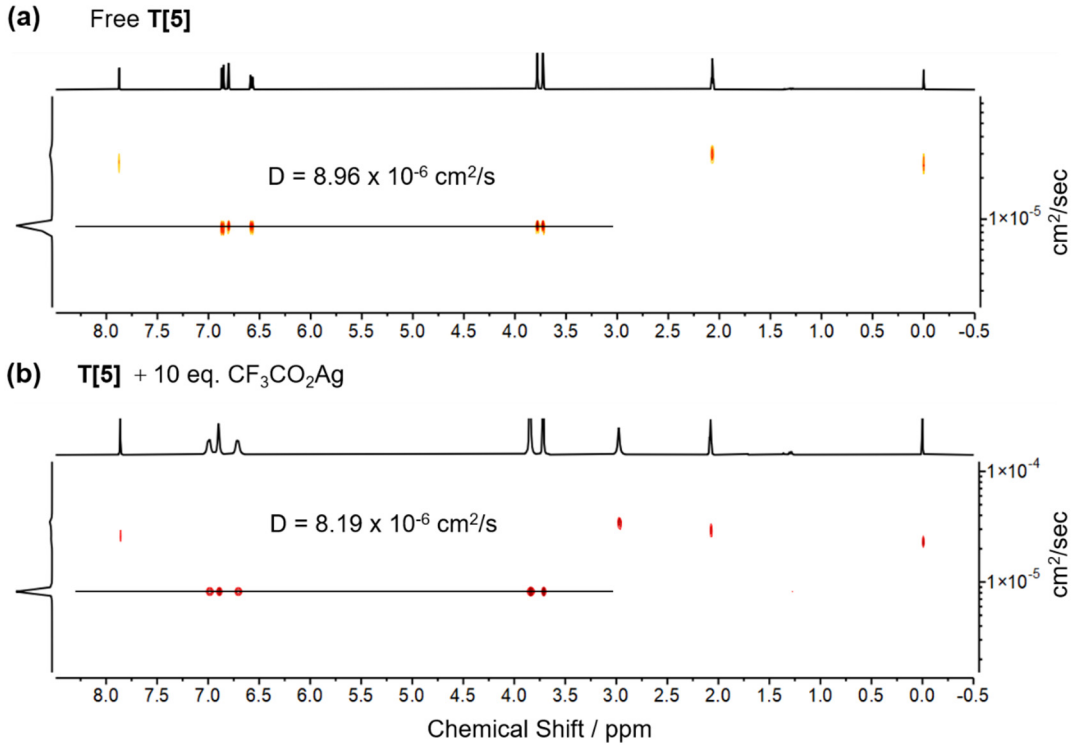

Figure S8. ^{1}H Diffusion-ordered spectroscopy (DOSY) spectra (400 MHz, $CDCl_3$: $(CD_3)_2CO$ = 1:2, *v*/*v*, 298 K) of (**a**) free **T[5]** and (**b**) the mixture of **T[5]** and 10 equiv. of CF_3CO_2Ag.

3. Mass Spectrometry Analysis

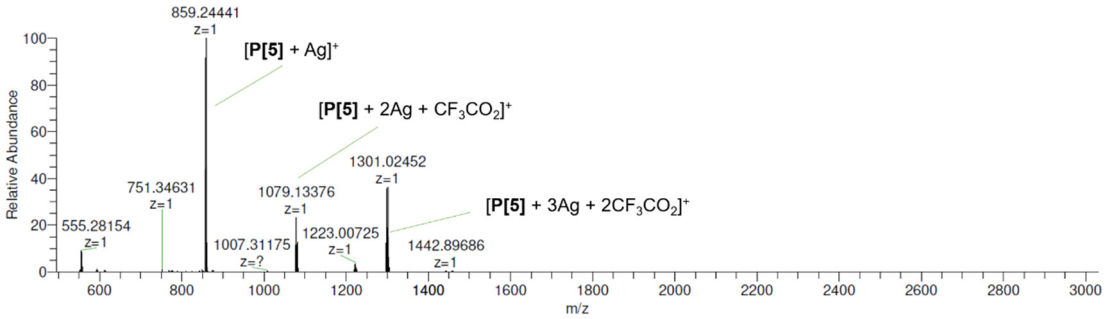

Figure S9. ESI-MS of the complex of **P[5]** and CF_3CO_2Ag. Assignment of main peaks: *m/z* [**P[5]** + Ag]$^+$ measured 859.24441, calc. 859.24461; [**P[5]** + 2Ag + CF_3CO_2]$^+$ measured 1079.13376, calc. 1079.13474; [**P[5]** + 3Ag + 2CF_3CO_2]$^+$ measured 1301.02452, calc. 1301.02453.

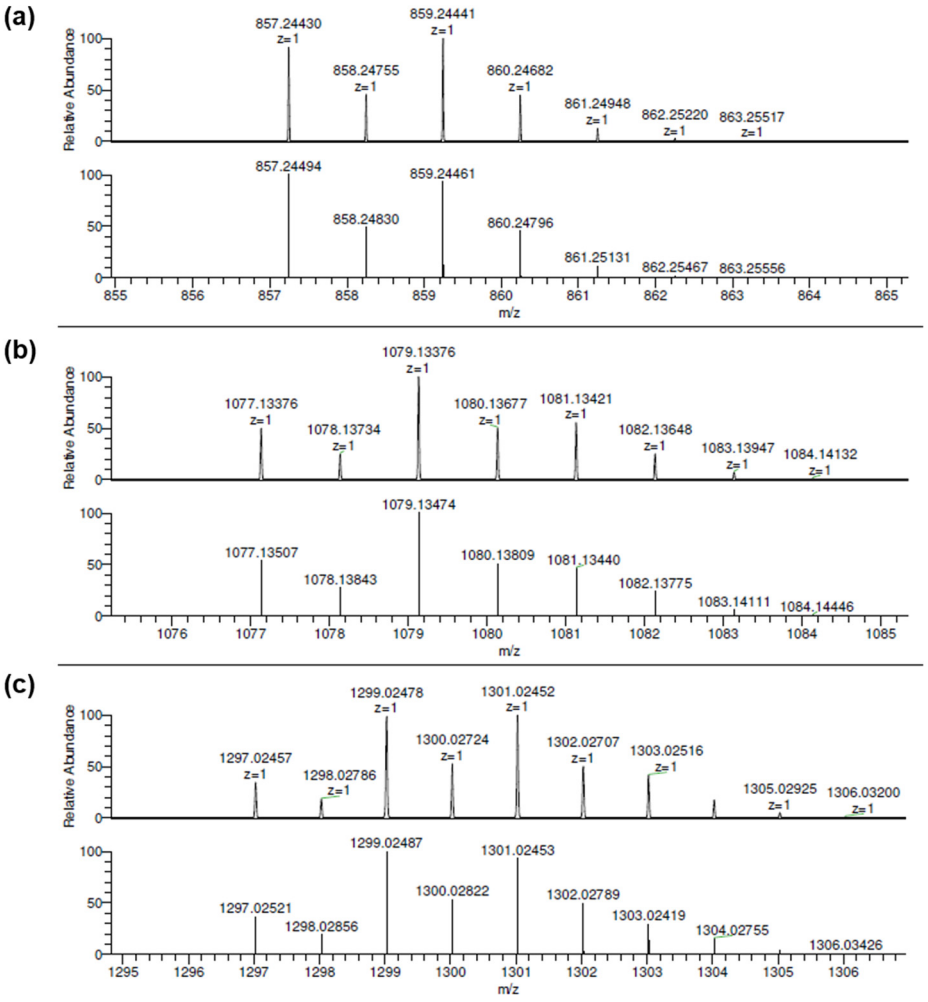

Figure S10. Experimental (top) and calculated (bottom) isotope patterns of a) [**P[5]** + Ag]$^+$; b) [**P[5]** + 2Ag + CF_3CO_2]$^+$; c) [**P[5]** + 3Ag + 2CF_3CO_2]$^+$.

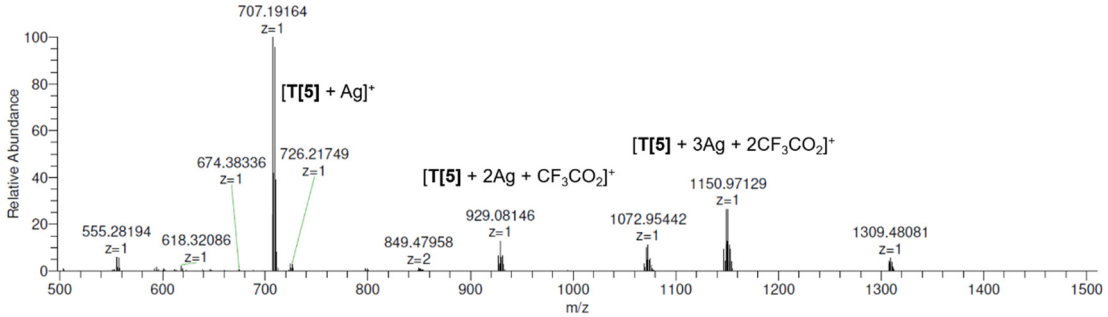

Figure S11. ESI-MS of the complex of **T[5]** and CF_3CO_2Ag. Assignment of main peaks: *m/z* [**T[5]** + Ag]$^+$ measured 709.19155, calc. 709.19178; [**T[5]** + 2Ag + CF_3CO_2]$^+$ measured 929.08146, calc. 929.08191; [**T[5]** + 3Ag + $2CF_3CO_2$]$^+$ measured 1150.97129, calc. 1150.97171.

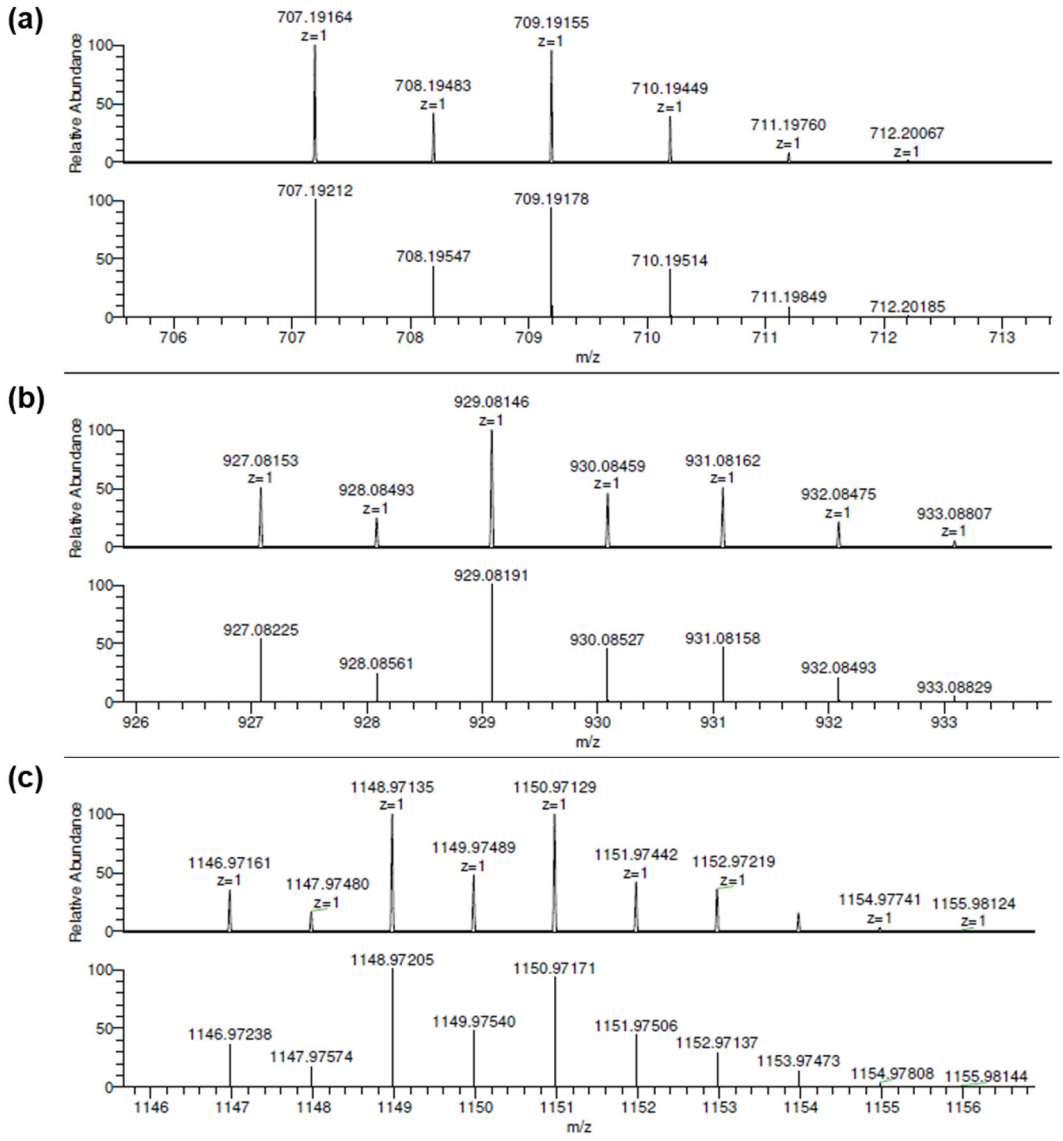

Figure S12. Experimental (top) and calculated (bottom) isotope patterns of a) [**T[5]** + Ag]$^+$; b) [**T[5]** + 2Ag + CF_3CO_2]$^+$; c) [**T[5]** + 3Ag + $2CF_3CO_2$]$^+$.

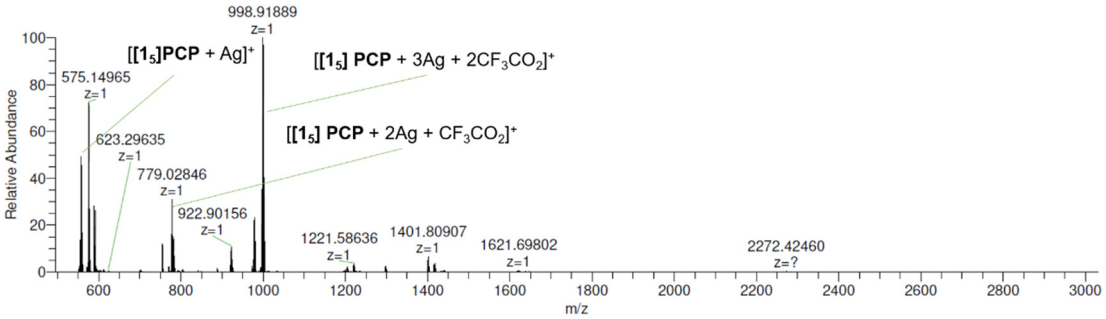

Figure S13. ESI-MS of the complex of **[1$_5$]PCP** and CF_3CO_2Ag. Assignment of main peaks: *m/z* [**[1$_5$]PCP** + Ag]$^+$ measured 559.13841, calc. 559.13896; [**[1$_5$]PCP** + 2Ag + CF_3CO_2]$^+$ measured 779.02846, calc. 779.02909; [**[1$_5$]PCP** + 3Ag + 2CF_3CO_2]$^+$ measured 998.91889, calc. 998.91922.

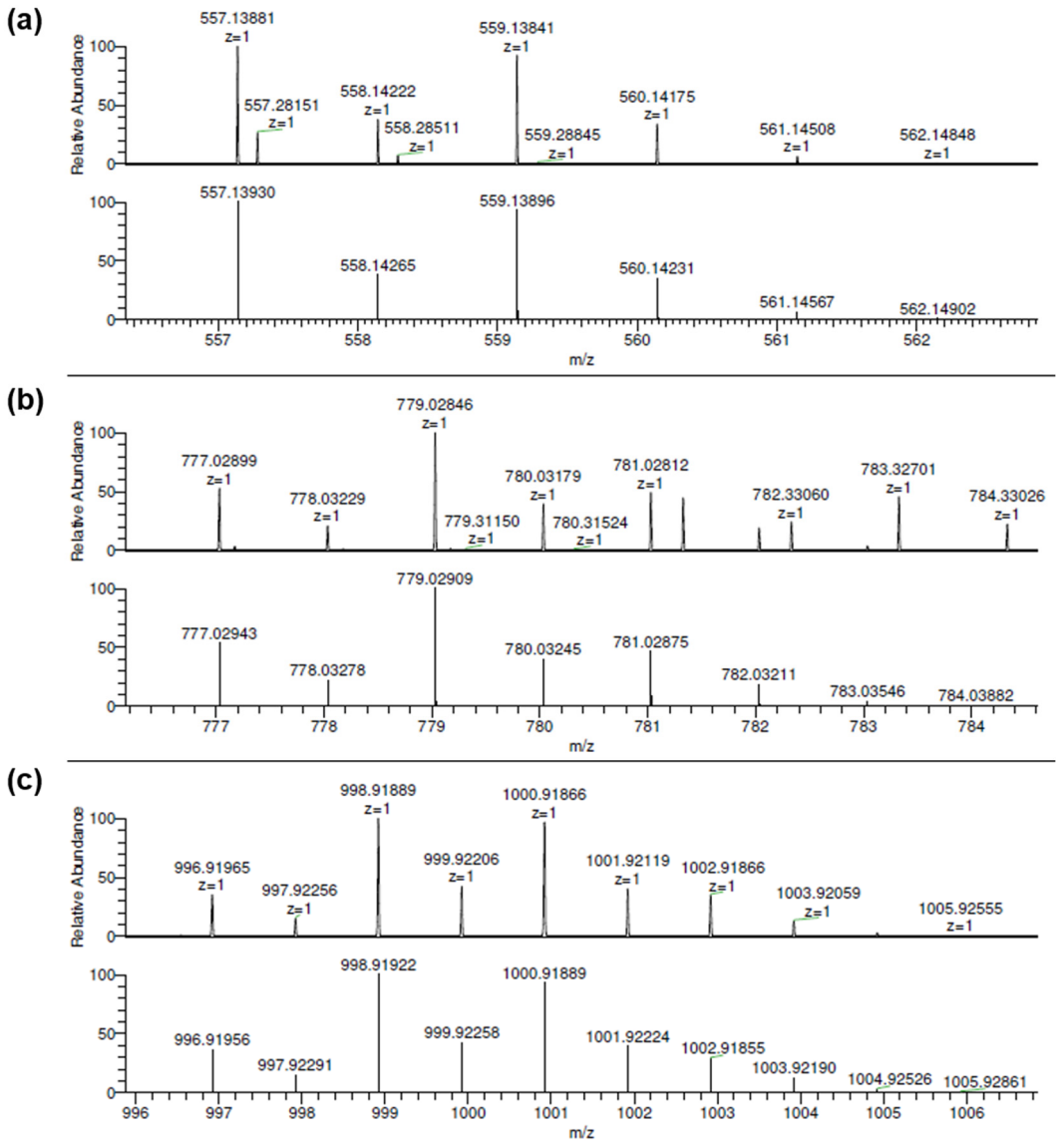

Figure S14. Experimental (top) and calculated (bottom) isotope patterns of a) [**[1$_5$]PCP** + Ag]$^+$; b) [**[1$_5$]PCP** + 2Ag + CF_3CO_2]$^+$; c) [**[1$_5$]PCP** + 3Ag + 2CF_3CO_2]$^+$.

4. Electrostatic Potential Maps

All calculations were performed with Gaussian 16 program package.[8] Based on density functional theory (DFT), geometry structures were given by single point calculation using the B3LYP−D3 functional[9] with the 6−311++G (d, p) basis set.[10] The visualization of the electrostatic potential (ESP) maps was created using the Multiwfn[11] and VMD[12] programs.

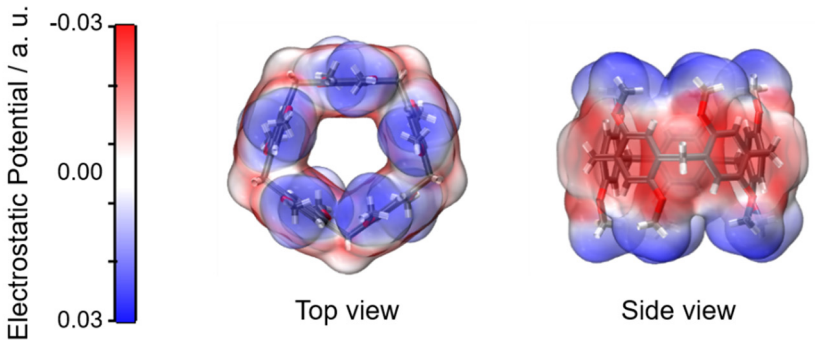

Figure S15. Calculated ESP maps for **P[5]**. Different colours indicate different electronegative regions. Red is the most nucleophilic and blue is the most electrophilic region.

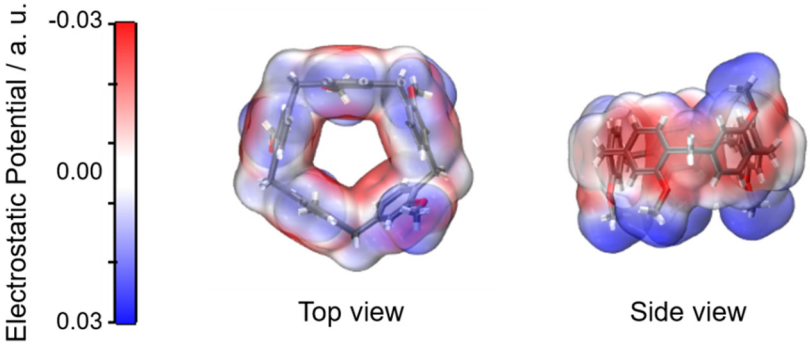

Figure S16. Calculated ESP maps for **T[5]**. Different colours indicate different electronegative regions. Red is the most nucleophilic and blue is the most electrophilic region.

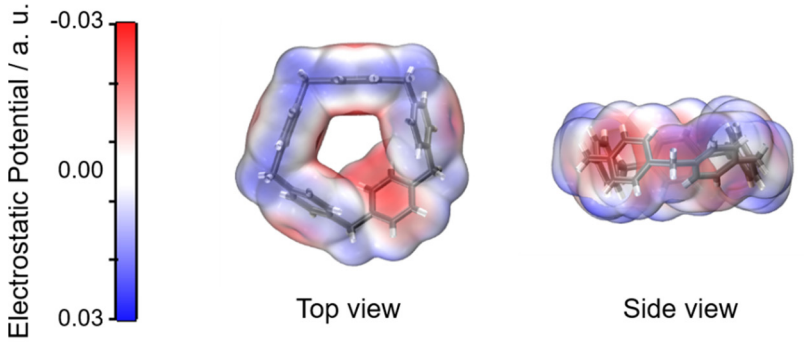

Figure S17. Calculated ESP maps for **[1$_5$]PCP**. Different colours indicate different electronegative regions. Red is the most nucleophilic and blue is the most electrophilic region.

5. X-Ray Crystallography

Table S1. Crystal data and structure refinement for ([$(CF_3CO_2Ag)_2$⊂**T[5]**])$_2$•$(CF_3CO_2Ag)_2$

Empirical formula	$C_{46}H_{40}Ag_3F_8O_{11}$
Formula weight / g mol^{-1}	1263.39
Temperature / K	160.00(10)
Crystal system	monoclinic
Space group	$P2_1/n$
a / Å	12.34190(10)
b / Å	20.96220(10)
c / Å	18.15160(10)
α / °	90
β / °	97.4690(10)
γ / °	90
Volume/ Å^3	4656.22(5)
Z	4
ρ_{calc} / g cm^{-3}	1.802
μ / mm^{-1}	10.875
F / 000	2504.0
2θ range for data collection / °	6.472 to 149.422
Crystal size / mm^3	0.02 × 0.02 × 0.02
Index ranges	$-15 \leqslant h \leqslant 15$, $-25 \leqslant k \leqslant 25$, $-19 \leqslant l \leqslant 22$
Reflections collected	62012
Independent reflections	9339 [$R_{int} = 0.0562$, $R_{sigma} = 0.0274$]
Data/restraints/parameters	9339/7/658
Goodness-of-fit on F^2	1.047
Final R indices [$I > 2\sigma(I)$]	$R_1 = 0.0610$, $wR_2 = 0.1581$
Final R indices [all data]	$R_1 = 0.0658$, $wR_2 = 0.1631$
Largest diff. peak / hole / e Å^3	1.85/-1.69
CCDC No.	2213177

Table S2. Crystal data and structure refinement for [$(CF_3CO_2Ag)_2$⊂(*M*)-**P[5]**]

Empirical formula	$C_{50}H_{51}Ag_2Cl_3F_6O_{14}$
Formula weight / g mol^{-1}	1331.99
Temperature / K	160.00(10)
Crystal system	orthorhombic
Space group	$P2_12_12_1$
a / Å	12.10780(10)
b / Å	20.0062(2)
c / Å	21.6776(2)
α / °	90
β / °	90
γ / °	90
Volume / Å^3	5250.99(8)
Z	4
ρ_{calc} / g cm^{-3}	1.660
μ / mm^{-1}	8.143
F / 000	2648.0
2θ range for data collection / °	6.012 to 147.484
Crystal size / mm^3	0.3 × 0.16 × 0.15
Index ranges	-14 ⩽ h ⩽ 14, -24 ⩽ k ⩽ 23, -22 ⩽ l ⩽ 26
Reflections collected	26674
Independent reflections	10225 [R_{int} = 0.0555, R_{sigma} = 0.0577]
Data/restraints/parameters	10225/8/706
Goodness-of-fit on F^2	1.032
Final R indices [I >2σ(I)]	R_1 = 0.0637, wR_2 = 0.1676
Final R indices [all data]	R_1 = 0.0661, wR_2 = 0.1713
Largest diff. peak / hole / e Å^3	2.00/-1.48
Flack parameter	-0.010(4)
CCDC No.	2213179

Table S3. Crystal data and structure refinement for [$(CF_3CO_2Ag)_2$⊂(*P*)-**P[5]**]

Empirical formula	$C_{50}H_{51}Ag_2Cl_3F_6O_{14}$
Formula weight / g mol^{-1}	1331.99
Temperature / K	159.99(10)
Crystal system	orthorhombic
Space group	$P2_12_12_1$
a / Å	12.1518(3)
b / Å	20.0181(5)
c / Å	21.6563(7)
α / °	90
β / °	90
γ / °	90
Volume / Å^3	5268.0(3)
Z	4
ρ_{calc} / g cm^{-3}	1.654
μ / mm^{-1}	8.116
F / 000	2648.0
2*θ* range for data collection / °	6.012 to 154.868
Crystal size / mm^3	0.1 × 0.1 × 0.05
Index ranges	$-15 \leqslant h \leqslant 15$, $-24 \leqslant k \leqslant 23$, $-18 \leqslant l \leqslant 27$
Reflections collected	29117
Independent reflections	10518 [R_{int} = 0.0903, R_{sigma} = 0.0767]
Data/restraints/parameters	10518/215/714
Goodness-of-fit on F^2	1.141
Final *R* indices [$I > 2\sigma(I)$]	R_1 = 0.0756, wR_2 = 0.2048
Final *R* indices [all data]	R_1 = 0.1050, wR_2 = 0.2271
Largest diff. peak / hole / e Å^3	1.23/-1.08
Flack parameter	-0.013(6)
CCDC No.	2213178

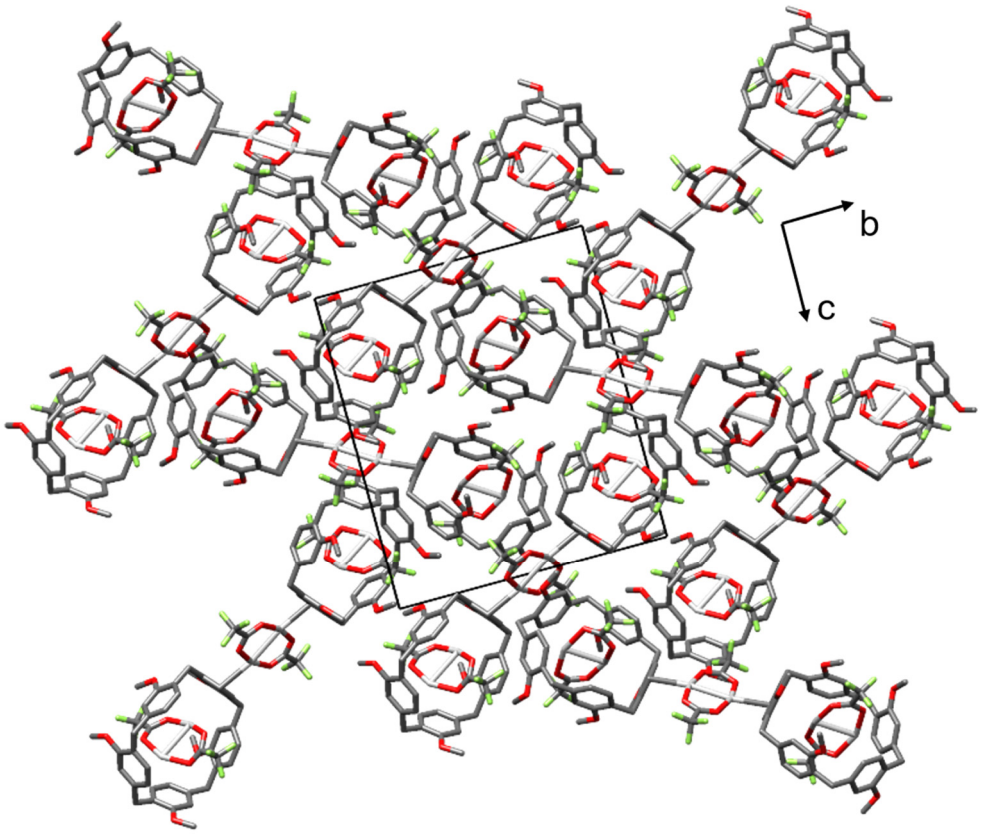

Figure S18. Unit cell and packing of $([(CF_3CO_2Ag)_2 \subset \mathbf{T[5]}])_2 \bullet (CF_3CO_2Ag)_2$ viewing from [100] direction. Hydrogen atoms are omitted for clarity.

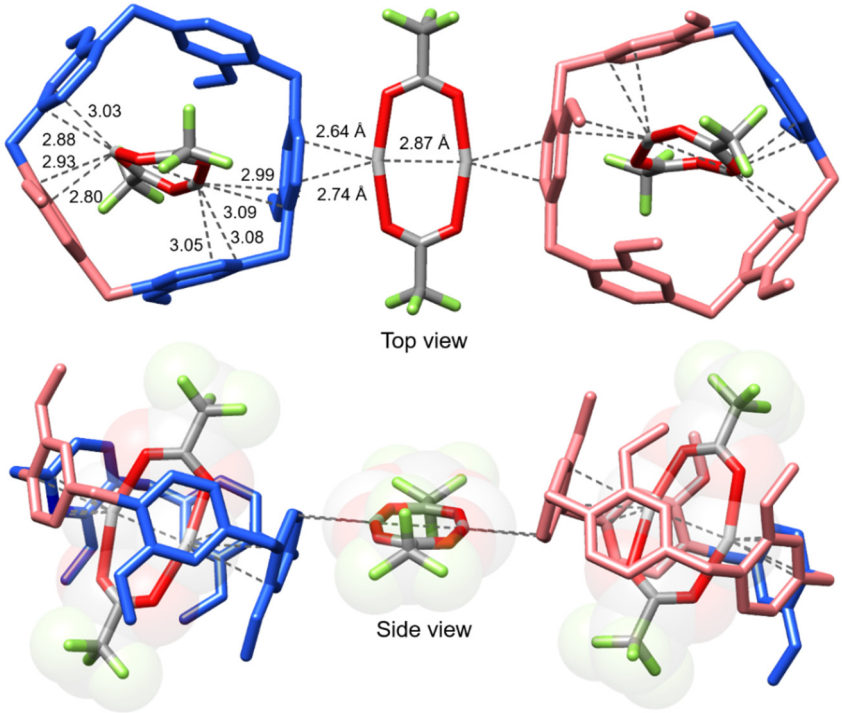

Figure S19. The handcuff-shaped structure of $([(CF_3CO_2Ag)_2 \subset \mathbf{T[5]}])_2 \bullet (CF_3CO_2Ag)_2$ with the Ag···π distances highlighted. Hydrogen atoms are omitted for clarity.

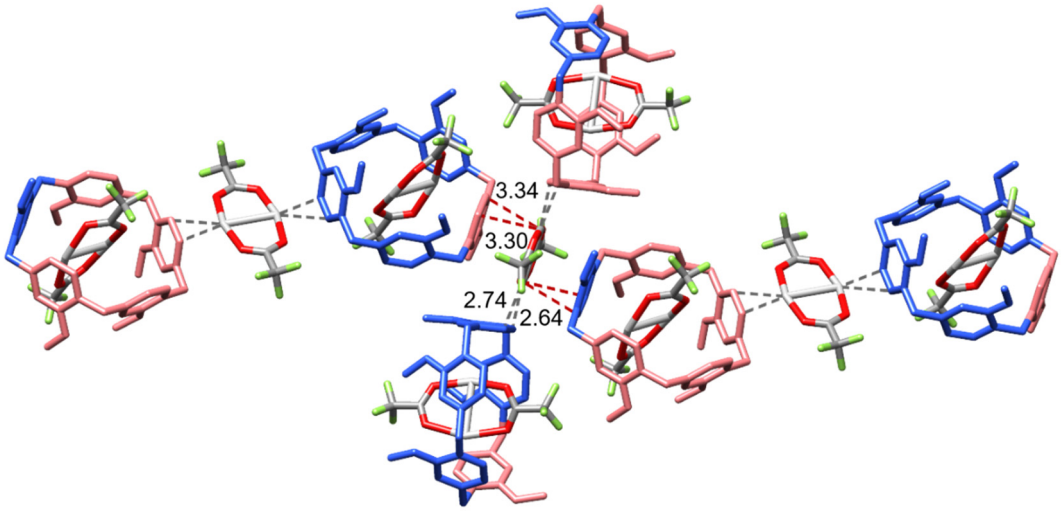

Figure S20. Partial crystal structure of $([(CF_3CO_2Ag)_2 \subset \mathbf{T[5]}])_2 \bullet (CF_3CO_2Ag)_2$ with the exo-wall Ag···C distances (Å) highlighted among handcuff-shaped structures (indicated by red dashed lines). Hydrogen atoms on the macrocycles are omitted for clarity.

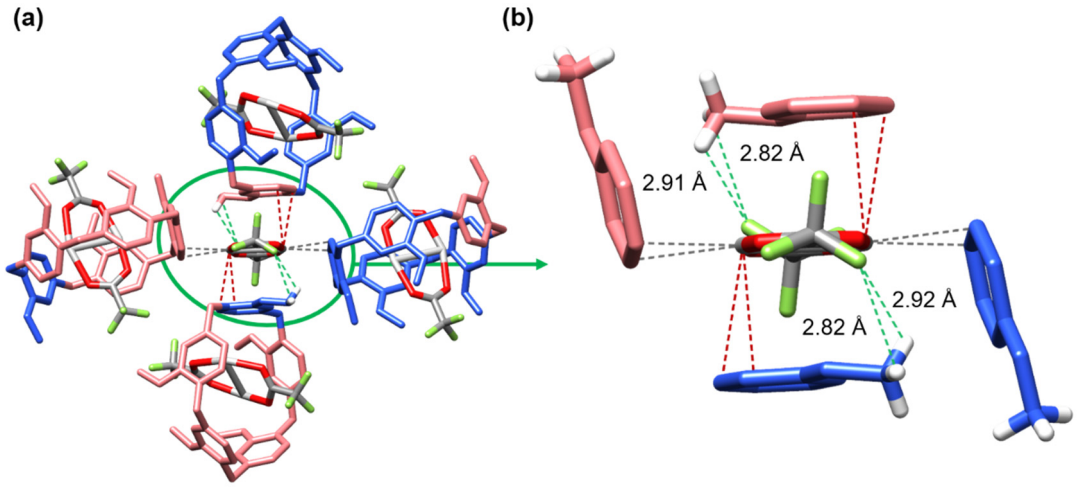

Figure S21. Partial crystal structure of $([(CF_3CO_2Ag)_2 \subset \mathbf{T[5]}])_2 \bullet (CF_3CO_2Ag)_2$ with the exo-wall C–H···F distances highlighted (indicated by green dashed lines). Hydrogen atoms not involved in C–H···F interactions are omitted for clarity.

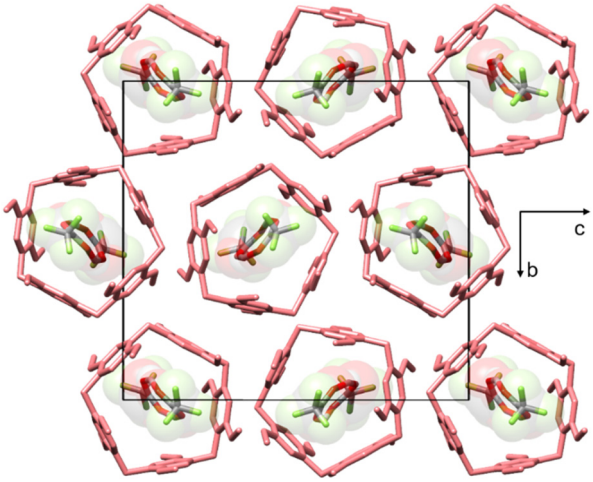

Figure S22. Unit cell of [$(CF_3CO_2Ag)_2$⊂(*M*)-**P[5]**] viewing from [100] direction. Hydrogen atoms are omitted for clarity.

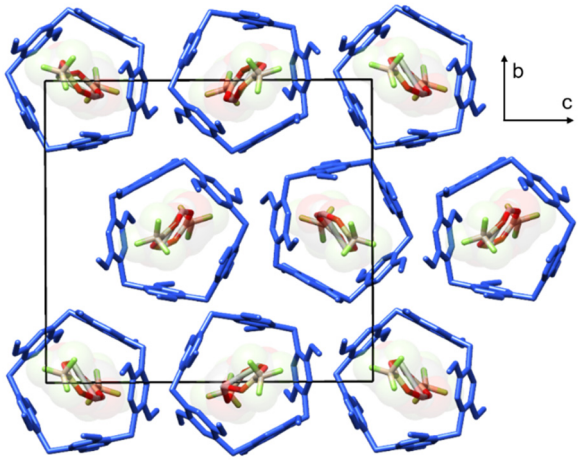

Figure S23. Unit cell of [$(CF_3CO_2Ag)_2$⊂(*M*)-**P[5]**] viewing from [100] direction. Hydrogen atoms are omitted for clarity.

6. Elemental Analysis

A vario EL CUBE elementar was used for the elemental analysis.

([$(CF_3CO_2Ag)_2$⊂**T[5]**])$_2$•$(CF_3CO_2Ag)_2$ complex:
Calc. (%) C = 43.74, H= 3.17; Found (%) C = 44.83, H = 3.42, N not found.

$(CF_3CO_2Ag)_2$⊂**P[5]** complex:
Calc. (%) C = 49.35, H= 4.20; Found (%) C = 43.37, H = 3.88, N not found.

7. Resolution by Triage

- Solid-State Electronic Circular Dichroism

Single crystals of the [$(CF_3CO_2Ag)_2$⊂**P[5]**] inclusion complex grown by slow solvent evaporation ($CHCl_3$/MeOH, *v*/*v* = 1:1) were picked by tweezers under a Leica DM2000 microscope with a polarized filter. Individual hexagonal prism single crystals were crushed into finely ground microcrystalline powder. Their KBr pellets were processed for solid-state electronic circular dichroism (ECD) measurements (Figure S24 and S25).

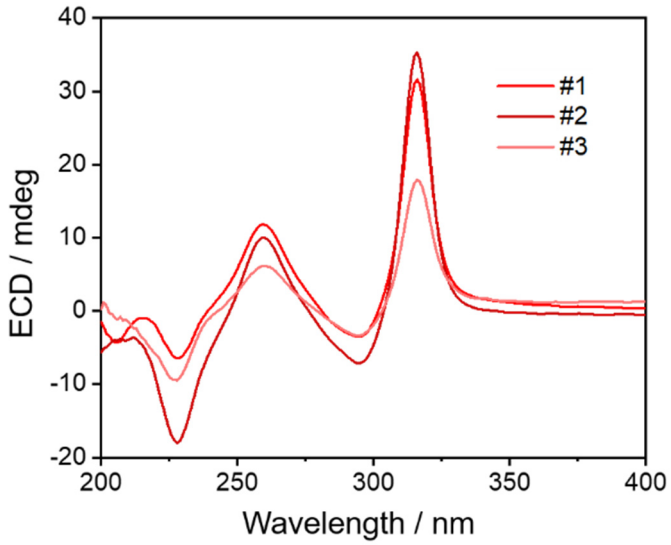

Figure S24. Solid-state ECD spectra of three different handpicked [$(CF_3CO_2Ag)_2$⊂(*M*)-**P[5]**] single crystals.

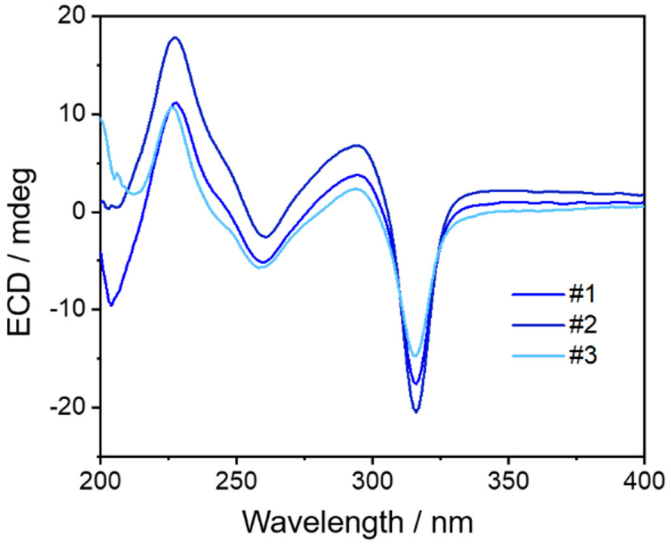

Figure S25. Solid-state ECD spectra of three different handpicked [$(CF_3CO_2Ag)_2$⊂(*P*)-**P[5]**] single crystals.

- Computational Electronic Circular Dichroism Spectra

Absorption energies were computed at TD-PBE0-D3(BJ)//PBE0-D3(BJ)/def2-SV(P) level of theory. Spectra were simulated from the excitation energies and rotation lengths by overlapping Gaussian functions for each transition, as implemented in the Multiwfn software.[11]

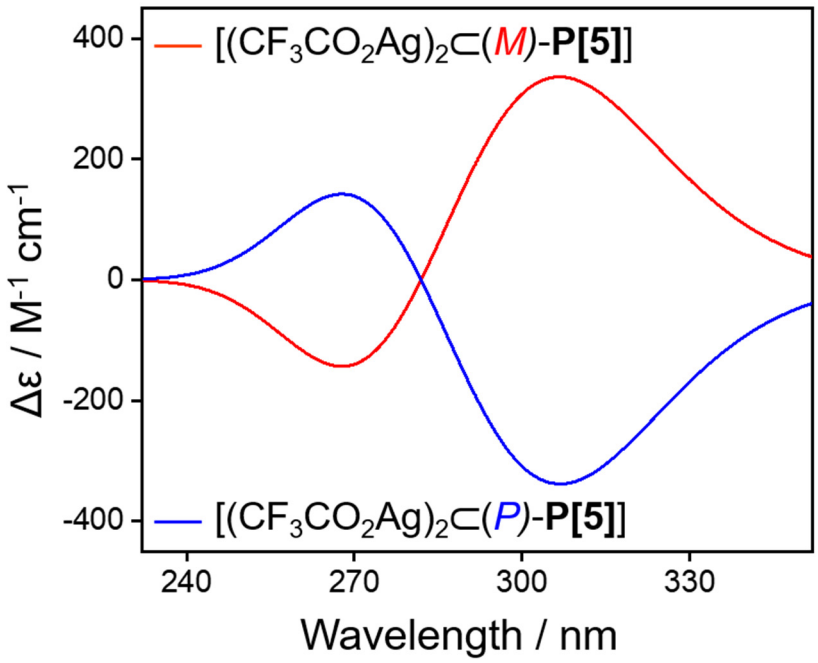

Figure S26. Simulated ECD spectra of [$(CF_3CO_2Ag)_2$⊂(*M*)/(*P*)-**P[5]**].

- Crystal Facet Indexing

Individual hexagonal prism-shaped [$(CF_3CO_2Ag)_2$⊂**P[5]**] single crystals were mounted on a Rigaku platform goniometer. The facets were indexed (Figure S27 and S28) by employing the Rigaku CryAlis Pro software. The results showed that the conglomerate crystals only feature holohedral faces (which have at least a zero in the miller indexes). Therefore, it is not possible to resolve the crystals of different handedness simply by comparing the crystal habits as Pasteur did for the sodium tartrates.

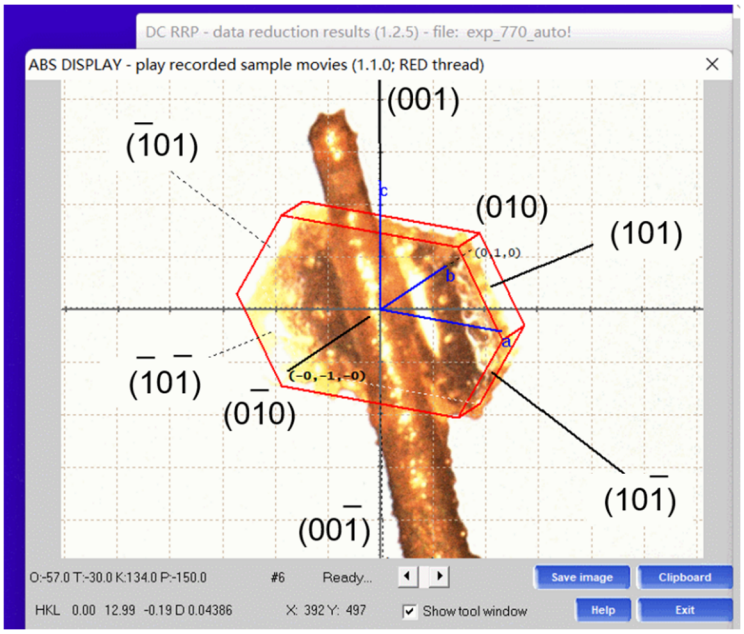

Figure S27. A representative screenshot used to index the facets of [$(CF_3CO_2Ag)_2$⊂**P[5]**] single crystal.

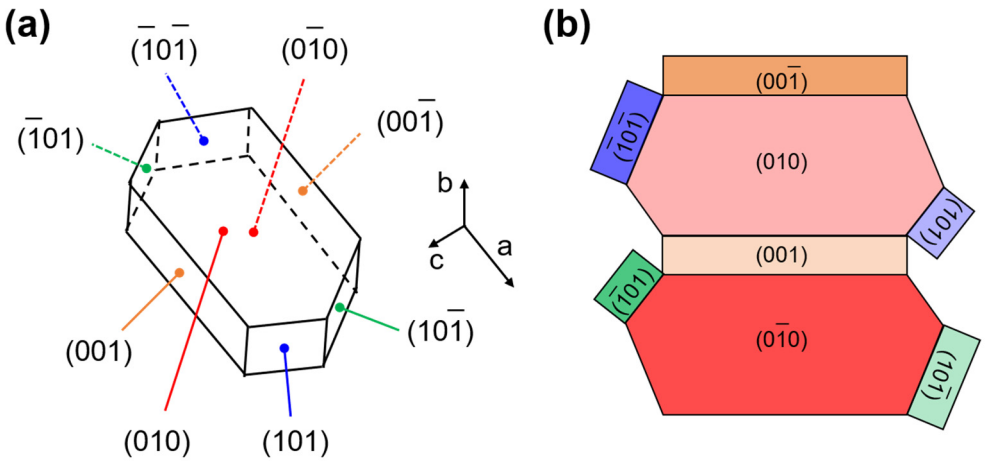

Figure S28. (a) The crystal habit of [$(CF_3CO_2Ag)_2$⊂**P[5]**] single crystal and (b) its corresponding 2D representation.

- Polarized Optical Microscopy

A transmission polarized optical microscope system with a CCD camera was used to examine [$(CF_3CO_2Ag)_2$⊂**P[5]**] single crystals. After slow evaporation of a $CHCl_3$/MeOH solution containing the mixture of CF_3CO_2Ag and **P[5]**, in addition to [$(CF_3CO_2Ag)_2$⊂**P[5]**] single crystals, individual **P[5]** crystals were also obtained in the mixture. Both types of crystals are colourless under the optical microscope (Figure S29a). When the mixture of crystals was placed between crossed polarizers, [$(CF_3CO_2Ag)_2$⊂**P[5]**] single crystals show (Figure S29b) either green or pink colours.

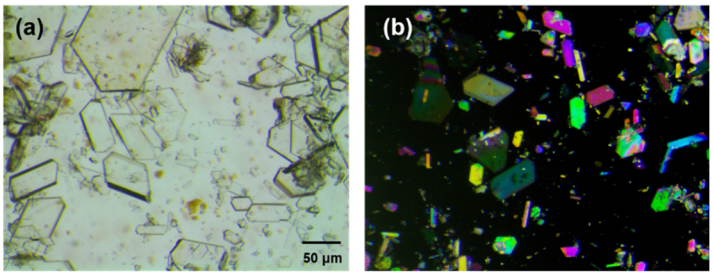

Figure S29. The snapshots of mixed single crystals viewed with (a) optical microscope and (b) crossed 90° polarisation.

Subsequently, two individual [$(CF_3CO_2Ag)_2$⊂**P[5]**] single crystals respectively showing green/pink colours between crossed polarizers were picked up. The crystals are both colourless without polarizer, but as the polarisers rotated from the parallel to the perpendicular position the colours of the two crystals show (Figure S30) gradual transitions from green to pink and pink to green, respectively.

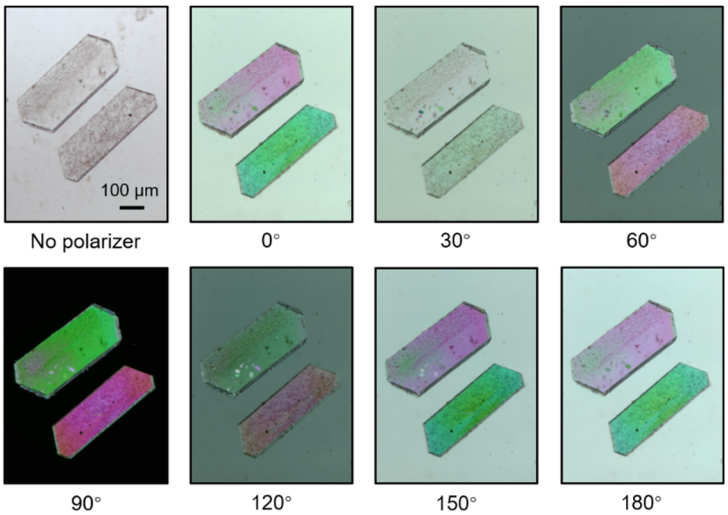

Figure S30. Colour transitions observed for [$(CF_3CO_2Ag)_2$⊂**P[5]**] crystals using polarised optical microscopy. Different colours appear when the analyser was rotated clockwise (angles indicated).

In order to identify the origin of the colour and whether the transition happens at a certain angle when rotating the polarizer, six more [$(CF_3CO_2Ag)_2$⊂**P[5]**] crystals of different thickness and sizes were analysed (Figure S31) using polarized microscope. The consistent colours shown by different crystals confirm that this effect is not related to interference. In addition, the colour transition happens at different rotating angles of the analyser for these crystals with different thickness.

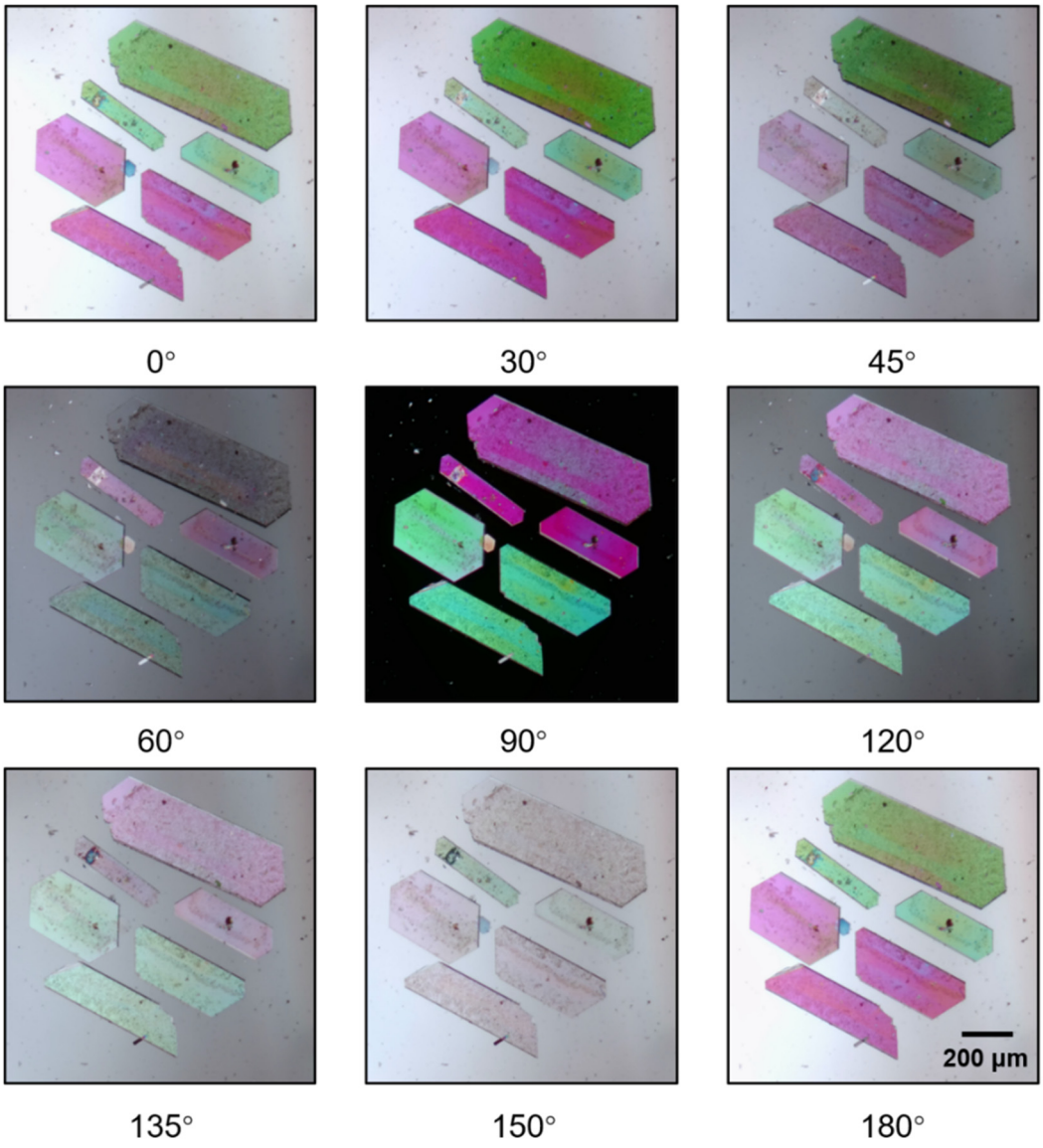

Figure S31. Colour transitions observed for [$(CF_3CO_2Ag)_2$⊂**P[5]**] crystals using polarised optical microscopy. Different colours appear when the analyser was rotated clockwise (angles indicated).

The observation of the different colours shown by [$(CF_3CO_2Ag)_2$⊂**P[5]**] single crystals under crossed polarizer prompted us to explore if the colours are related to the handedness of the crystals.[13]

Under crossed 90° polarization, 10 crystals showing green (Figure S32) and 10 crystals showing red (Figure S34) were respectively handpicked and processed for solid-state electronic circular dichroism (ECD) measurements. Nonetheless, the signs of the Cotton effect observed (Figure S33 and S35) are independent of the colour of the crystals. In other words, we were unable to distinguish *P* and *M*-crystals by simply comparing the crystal colours under polarized microscope. The results were further verified (Table S4) by X-ray crystallography.

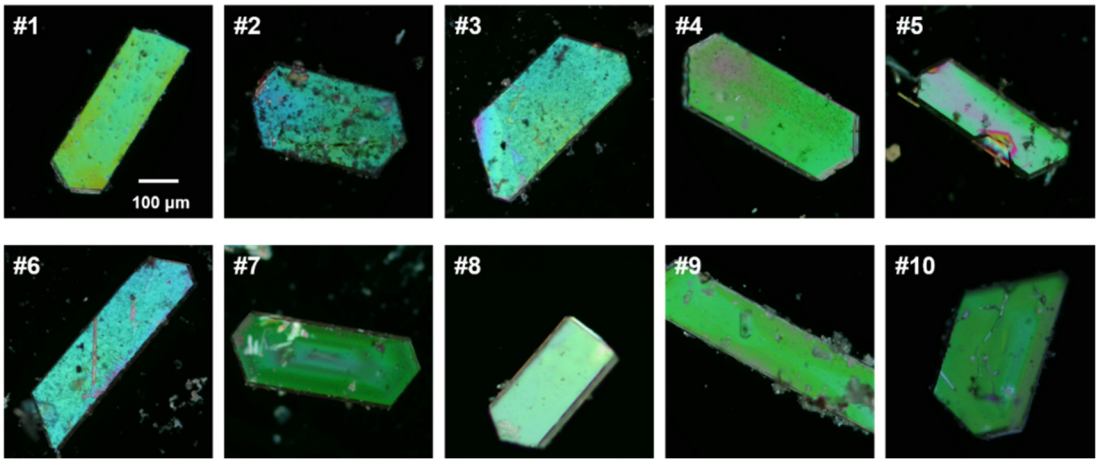

Figure S32. The snapshots of 10 different handpicked [$(CF_3CO_2Ag)_2$⊂**P[5]**] single crystals which show green colour viewed under crossed polarizers.

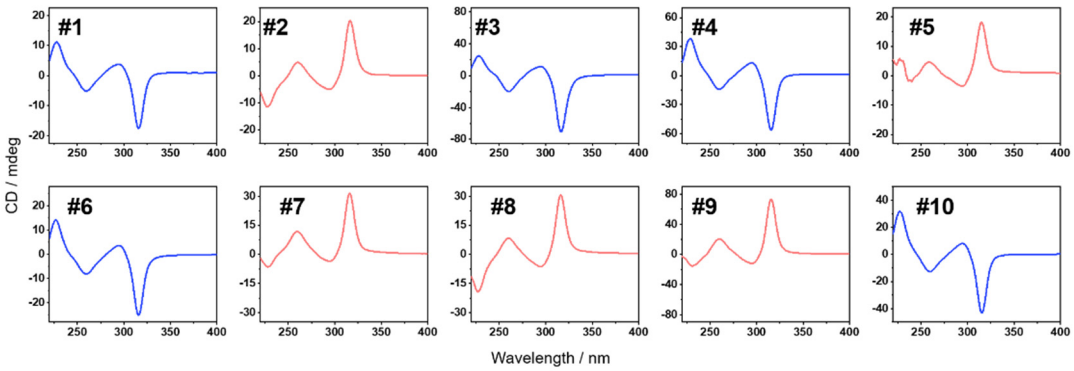

Figure S33. Solid-state ECD spectra of 10 different handpicked [$(CF_3CO_2Ag)_2$⊂**P[5]**] single crystals which show green colour viewed under crossed polarizers.

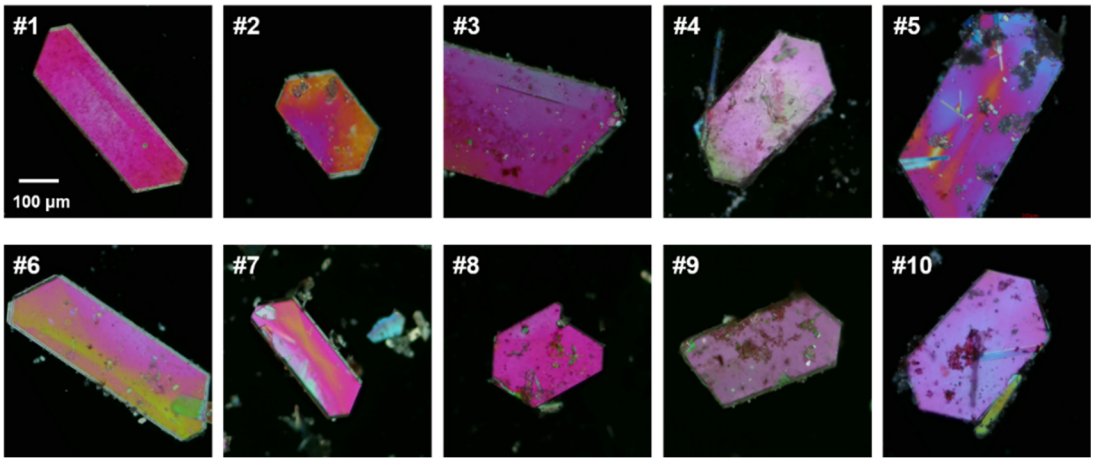

Figure S34. The snapshots of 10 different handpicked [$(CF_3CO_2Ag)_2$⊂**P[5]**] single crystals which show pink colour viewed under crossed polarisers.

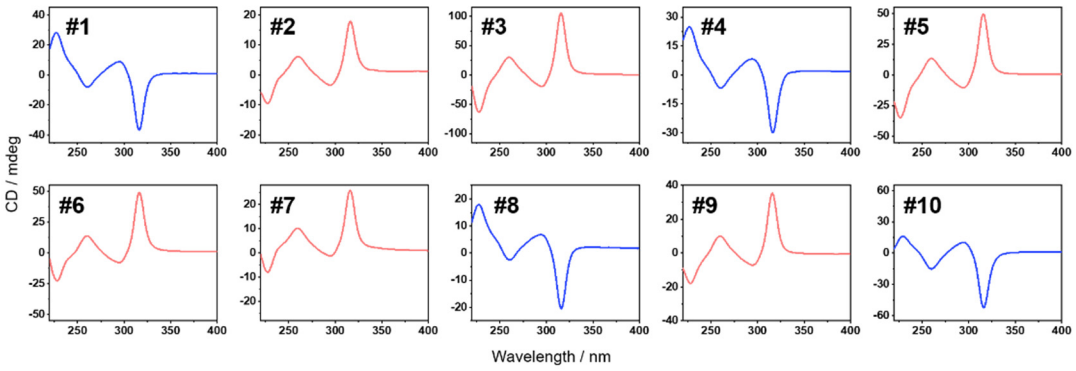

Figure S35. Solid-state ECD spectra of 10 different handpicked [$(CF_3CO_2Ag)_2$⊂**P[5]**] single crystals which show pink colour viewed under crossed polarisers.

Table S4. The Flack parameters of 8 individual [$(CF_3CO_2Ag)_2$⊂**P[5]**] crystals

Sample Number	Colour under Crossed Polarizers	Space Group	Handedness	Flack Parameter
1	green	$P2_12_12_1$	*M*-	-0.005(5)
2	green	$P2_12_12_1$	*P*-	-0.009(4)
3	green	$P2_12_12_1$	*M*-	0.021(4)
4	green	$P2_12_12_1$	*M*-	0.003(5)
5	pink	$P2_12_12_1$	*M*-	-0.008(9)
6	pink	$P2_12_12_1$	*P*-	0.064(5)
7	pink	$P2_12_12_1$	*M*-	0.001(5)
8	pink	$P2_12_12_1$	*P*-	0.088(5)

8. References

1. G. M. Sheldrick, *Acta Cryst. Sect*., 2015, **C71**, 3.
2. G. M. Sheldrick, *Acta Cryst. Sect.*, 2008, **A64**, 112.
3. O. V. Dolomanov, L. J. Bourhis, R. J. Gildea, J. A. K. Howarda and H. Puschmann, *J. Appl. Cryst.*, 2009, **42**, 339.
4. T. Ogoshi, T. Aoki, K. Kitajima, S. Fujinami, T. Yamagishi and Y. Nakamoto, *J. Org. Chem*., 2011, **76**, 328.
5. W. Yang, K. Samanta, X. Wan, T. U. Thikekar, Y. Chao, S. Li, K. Du, J. Xu, Y. Gao, H. Zuilhof and A. C.-H. Sue, *Angew. Chem. Int. Ed.*, 2020, **59**, 3994.
6. P. Liu, Q. Li, H. Zeng, B. Shi, J. Liu and F. Huang, *Org. Chem. Front.*, 2019, **6**, 309.
7. P. Thordarson, *Chem. Soc. Rev.*, 2011, **40**, 1305.
8. M. J. Frisch, et al. *Gaussian 16 Rev.*, A.03, Wallingford, CT, 2016.
9. (*a*) A. D. Becke, *J. Chem. Phys.*, 1993, **98**, 5648; (*b*) C. Lee, W. Yang and R. G. Parr, *Phys. Rev. B*, 1988, **37**, 785; (*c*) A. D. Becke, *J. Chem. Phys.,* 1993, **98**, 1372.
10. R. Krishnan, J. S. Binkley, R. Seeger and J. A. Pople, *J. Chem. Phys*., 1980, **72**, 650.
11. T. Lu and F. Chen, *J. Comput. Chem.,* 2012, **33**, 580.
12. W. Humphrey, A. Dalke and K. Schulten, *J. Molec. Graphics*, 1996*,* **14**, 33.
13. (*a*) L. Koby, J. B. Ningappa, M. Dakessian and L. A. Cuccia, *J. Chem. Educ.*, 2005, **82**, 1043; (*b*) J.-M. Cruz, K. Hernández-Lechuga, I. Domínguez-Valle, A. Fuentes-Beltrán, J. U. Sánchez-Morales, J. L. Ocampo-Espindola, C. Polanco, J.-C. Micheau and T. Buhse, *Chirality*, 2020, **32**, 120.